journal

J. Am. Ceram. Soc., 91 [11] 3643–3651 (2008)
DOI: 10.1111/j.1551-2916.2008.02619.x

Atomistic Simulation of Y-Doped α-Alumina Interfaces

Sandra Galmarini, Ulrich Aschauer,† and Paul Bowen

Laboratoire de technologie des poudres, Ecole polytechnique fédérale de Lausanne, 1015 Lausanne, Switzerland

Stephen C. Parker

Department of Chemistry, University of Bath, Bath BA2 7AY, U.K.

The exact mechanism of creep resistance enhancement due to yttrium (Y) doping in α-alumina is still subject to speculation, although it is known that dopants segregate strongly to grain boundaries. The current work applies atomistic simulation techniques to the study of segregation to a reasonable number of interfaces in Y-doped α-alumina. Y is shown to segregate stronger to surfaces than grain boundaries and to form ordered structures at the interfaces, which may decrease diffusion coefficients. These Y-ordered regions may act as nucleation sites for YAG precipitates particularly for rapid sintering techniques.

I. Introduction

YTTRIUM (Y) dopants added to α-alumina (α-Al_2O_3) enhance the creep resistance at high temperatures,[1,2] making it a common dopant in laboratory and industrial applications. The underlying atomic scale mechanisms are, however, still speculated upon, the following literature review showing possible explanations for this so-called Y effect. It is well known that Y strongly segregates to α-alumina surfaces and that its solubility in the bulk is very limited (~10 atomic ppm).[3,4] Imaging-SIMS confirmed Y dopants in α-alumina ceramics to be located mainly at grain boundaries and free surfaces in pores.[5] The creep resistance was shown to be dependent on the Y dopant concentration until the α-alumina phase is saturated and precipitation of yttrium–aluminum–garnet particles (YAG, $Y_3Al_5O_{12}$) occurs.[2] Energy dispersive X-ray spectrometry (EDX)[6,7] and X-ray adsorption fine structure (EXAFS)[8] studies have shown the Y grain-boundary concentration to increase with increasing bulk concentration up to a supersaturation of 5–9 Y/nm^2. Following the precipitation of YAG particles, the Y grain-boundary concentration decreases to an equilibrium concentration of 3–7 Y/nm^2. Further addition of Y only increases the number of YAG particles without affecting the creep resistance. This indicates that the creep resistance of α-alumina is increased by Y dopants in solid solution rather than by the presence of YAG particles.

The microstructure was shown to be almost unaffected by the presence of Y in solid solution. The fraction of special grain boundaries, i.e., coincidence site lattice (CSL) and near-CSL grain boundaries, does not change significantly with the presence of Y dopants (<5% for both Y-doped and pure α-alumina).[9] Also the Y dopants in solid solution do not seem to limit grain growth and the grains remain equiaxed,[6,7] however, the densification is retarded.[10] There seem to be many grain boundaries parallel to the (00.1) or the (01.2) plane of one of the adjacent half-crystals[6,11,12] which has also been observed for an Mg, Ti codoped α-alumina.[13]

As microstructure modification does not seem to be the reason behind creep suppression, recent research has focused on the interaction of Y ions with grain boundaries and dislocations. Several authors used X-ray absorption near edge structure and EXAFS to obtain additional information about the atomic environment of Y ions segregated to grain boundaries.[8,14,15] At low concentrations the Y ions take positions in the grain-boundary core whereas with increasing Y concentration a near boundary layer is formed and the structures relax to O–Y distances similar to those found in Y_2O_3 reflecting the lower bond strength for Y–O as compared with Al–O.[8] These measurements characterize the global properties of a material with many different grain boundaries and are thus not easy to correlate with other studies investigating isolated and often special bicrystal grain boundaries by methods such as high-resolution transmission electron microscopy (HRTEM), high-angle annular dark field transmission electron microscopy,[16,17] and electron energy loss spectroscopy (EELS). The studies of isolated grain boundaries show that the Y concentration varies from grain boundary to grain boundary and sometimes even along one and the same grain boundary. The change in bonding environment found by EELS[18,19] and confirmed by quantum mechanical cluster calculations[20,21] is assumed to contribute to the creep reducing effect by influencing the transport properties in the segregated layer close to the grain boundary.

As twin boundaries are readily accessible to computer simulations, a large variety of boundary types has been investigated using atomistic simulation methods based on empirical pair potentials[22–27] as well as electronic structure methods.[16,27–31] The pristine boundaries investigated were for the most part special boundaries, however, some cases with Σ values up to 39 can be considered as general grain boundaries. The structures found in these theoretical studies correlated well with experimental HRTEM investigations[29] as did the grain-boundary energies when compared with thermal grooving experiments.[32]

The role of Y dopant ions and their segregation has been investigated by classical[23,33] as well as density functional theory methods.[34–37] All authors agree on the fact that the Y dopant atoms segregate toward grain boundaries. In classical simulations the Σ13 (10.4) boundary exhibited the lowest driving force for segregation with 0.71 eV for the first ion and 0.87 eV for the second ion, suggesting an interaction between the dopant ions.[23] The *ab initio* approach[34] gives segregation energies between 1 and 3 eV for a single Y ion in a Σ7 (10.2) boundary depending on the location of the dopant in the structure. Segregation toward the Σ3 (10.0) and Σ13 (10.4) boundaries was investigated as well, the latter being considered near general, finding segregation energies of 1.01 and 2.3 eV per Y ion, respectively.[35] Segregation of the second ion was found to be more favorable for the Σ3 and Σ7 boundaries, whereas for the Σ13 case the synergetic interaction between dopants was not observed. Further research showed that the favorable interaction between Y ions only takes place upon structural relaxation, resulting in a gain of about 0.3 eV per dopant ion pair.[36]

G. S. Rohrer—contributing editor

Manuscript No. 24340. Received February 21, 2008; approved June 29, 2008.
This work was financially supported by the European Sixth Framework Integrated Project Nanoker No. NMP3-CT-2005-515784.
†Author to whom correspondence should be addressed. e-mail: uli.aschauer@epfl.ch

Electronic structure methods are generally assumed to be more precise, however, at a much higher computational cost and limited by the number of atoms which can be treated. This very often leads to extremely small simulation cells, where the interaction between periodic images of boundaries and dopant ions in the structure is probably not negligible. The potential-based method was shown to qualitatively give the same results as the more expensive density functional theory approach even if the energies and structures showed slight variations.[16,27] Potential-based methods therefore still have a merit compared with the so-called "state-of-the-art" simulation methods, when it comes to looking at larger cells and more structures. If the results obtained with empirical potentials can be validated against *ab initio* methods for some structures, potential-based methods can therefore be used to bridge the gap between the highly precise but small-scale *ab initio* methods and experimental investigations of real grain boundaries in ceramic materials.

The cited *ab initio* studies showed a highly specific segregation behavior for each interface, making it necessary to calculate a large range of interfaces in order to get the general trend as it would be observed in a ceramic material. This goal is pursued in the context of the current work where a large number of Y-doped α-alumina interfaces, surfaces as well as grain boundaries, have been studied by means of energy minimization based on classical empirical potentials. The study of a large number of interfaces—some having big interface areas and thus many atoms—over a wide range of doping concentrations is, at least at the present time, not possible with first principle methods. The method applied in the present work may therefore be able to bridge the gap between the characterization of isolated grain boundaries and experimental observations on a material with a statistical distribution of different grain boundaries.

II. Experimental Procedure

Calculations were made with the METADISE code,[38] which implements an energy minimization technique based on classical potential models, describing the potential energy using relatively simple analytical functions of the relative atomic positions. The potential set employed in this work[39] is a simple pair potential expressing the interaction (V_{ij}) between two atoms of a certain type (atoms i and j) as a function of the distance (r_{ij}) between those two atoms. It takes into account coulombic (first term in Eq. (1)) and both repulsive and attractive short-range contributions (second and third term of Eq. (1), respectively).

$$V_{ij}(r_{ij}) = V_{\text{Coulomb}} + V_{\text{disp}} = \frac{q_i q_j}{r_{ij}} + A_{ij} e^{-\frac{r_{ij}}{\rho_{ij}}} - \frac{C_{ij}}{r_{ij}^6} \quad (1)$$

where q is the charge of the respective ion and A_{ij}, ρ_{ij}, and C_{ij} are constants fitted to experimental data such as the lattice and elastic constants. Polarizability of the oxygen ion is taken into account by a core–shell model as described by Dick and Overhauser,[40] in which an ion is split into a core and a massless shell, carrying together the net charge of the ion. The core (c) and the shell (s) are held together by a harmonic spring potential (V_{cs}) as given in the following equation:

$$V_{cs}(r_{cs}) = \tfrac{1}{2} k_{cs} r_{cs}^2 \quad (2)$$

where r_{cs} is the distance between the core and the shell and k_{cs} is a constant determining the core–shell separation in a given electric field and thus the resulting dipole moment. The interactions coming from surrounding atoms are applied on the shell. This potential approach has been validated for segregation to surfaces in α-Al_2O_3[41] as well as more recently to the isostructural hematite.[42] The total energy of the system is calculated by summing the interactions between all pairs of atoms up to a cutoff radius of 15 Å.

A potential set is a relatively simple description of atomic interactions as opposed to *ab initio* methods, which calculate the interactions via approximate solutions to the quantum mechanical Schrödinger equation and can thus account for changes in the bonding character; however, with consequence of much longer calculation times. Wilson *et al.*[43] have shown that simple shell models can favor the stability of Al_2O_3 phases other than α. It is therefore important to validate the equilibrium bulk structure predicted by the potential model by comparison with known experimental values as given in Table I. The match is fair, however, far from perfect. The elastic constants are systematically overestimated whereas the dielectric constants are underestimated, these slight variations may be attributable to the fact that the calculated properties are considered without a thermal contribution and not at ambient temperature as for the measured properties. A slight shrinkage along the c-axis is observed, the lattice energy, however, matches very well. The model thus seems to produce the α-phase reasonably well, however, not as accurately as *ab initio* or quadrupolar potential models. The employed potential model, however, was found to work well in under-coordinated environments where other models[44] showed anomalous relaxations. Another important point to note is that the multipole moments are known to play an important role in highly symmetrical systems, whereas for low symmetry systems the dipolar approximation is sufficient.[45,46] As grain boundaries are not of high symmetry, their atomic structures should be reproduced with reasonable accuracy by shell models.

Energy minimization is a method adapting the atomic coordinates to iteratively converge toward the atomic configuration with minimum total energy. A preminimization of 10 conjugate gradient steps has been applied followed by the Newton–Raphson method until convergence. Depending on the initial atomic positions this method is always at risk to find local minima, thus often several initial configurations have to be tested in order to increase the chances of finding a physically meaningful minimum. Energy minimization cannot describe temperature effects or entropic contributions as other methods such as molecular dynamics simulations do.

In order to describe an interface separating two otherwise infinite half-crystals, periodic boundary conditions have been applied in the interface plane only. Along the direction normal to the interface the structure has been divided in two regions, atoms in the region adjacent to the interface were allowed to relax to their minimum energy position whereas atom in the region further away from the interface were fixed at their perfect single crystal positions. The depth of the surface region is chosen for complete relaxation of the surface to be possible without restriction due to the fixed region ($\geq$ 16.2 Å). Complete relaxation also has to be ensured when dopants are inserted at the maximum simulated depth. The bulk region has to be deep enough to make long-range coulombic interaction between its

Table I. Comparison Between Experimental Properties (Lattice Constants from Liu *et al.*[58] Elastic Constants and Lattice Energy from Handbook of Chemistry and Physics,[59]) and those Predicted by the Model

	A (Å)	c (Å)	ε_{11} (—)	ε_{33} (—)	C_{11} (GPa)	C_{12} (GPa)	C_{13} (GPa)	C_{33} (GPa)	C_{44} (GPa)	U_{pot} (kJ/mol)
Experiment	4.76	12.99	9.34	11.54	497.35	163.97	112.20	449.11	147.39	−15916
Simulation	4.72	12.43	8.24	12.52	666.09	269.10	191.59	519.88	157.96	−15533

As it can be seen the properties are reasonably well reproduced. Moreover this potential model was found to reproduce under-coordinated environments such as surfaces and grain boundaries without anomalous relaxations.

top and bottom atoms negligible ($\geq$ 80 Å). This model is valid for grain sizes where an unperturbed bulk structure exists at the core. For the simulation of nanomaterials, where interfaces interact with one another, the rigid zone could be reduced and a second surface layer added at the opposite side—however, the surface region depth would most likely have to be increased as well. All simulated grain boundaries were mirror twin and consequently CSL grain boundaries, although high grain-boundary energies and high Σ values indicate an almost general character for some boundaries. For surfaces as well as grain boundaries several nonpolar cuts at different depths along the same surface normal have been calculated, the final structure corresponding to the termination with the lowest energy. For grain boundaries the optimal rigid shift in the grain-boundary plane has been determined by moving the two adjoining half-crystals in a grid-like fashion in steps of 0.2 Å with respect to each other and performing an energy minimization for each grid point. The structure of the grain boundary corresponds to the relative position of the two half crystals having a minimum energy.

Once the structure of the pristine interface had been calculated, more and more aluminum ions have been substituted by Y ions. For each interface concentration several initial positions of the Y atoms have been considered—the exact number is highly dependent on surface structure and concentration ranging from 1 (when all surface atoms are replaced) to over 50 possibilities for the larger grain boundaries. The interface energy γ has been calculated as given in Eq. (3), where E_{interf} is the energy of the doped interface, E_{bulk} the energy of the same number of atoms (N_{Al}, N_{O}, and N_{Y}) in the bulk and A_{interf} the area of the simulated interface. The interface energy can also be expressed as a function of the free energy change when cleaving the undoped crystal ($\Delta G_{\text{interf},\Gamma_{\text{Y}}=0}$)and the formation energy of N_{Y} substitutional Y defects at the interface ($\Delta E^{\text{interf}}_{\text{defect,Y}}$) and in the bulk ($\Delta E^{\text{bulk}}_{\text{defect,Y}}$) respectively. As the first part of the expression is equivalent to the undoped interface energy ($\gamma_{\Gamma_{\text{Y}}=0}$) and the difference in formation energies is the driving force for segregation ($\Delta H_{\text{seg,Y}}$) the surface energy can be written as a function of these readily accessible quantities and the interfacial dopant concentration (Γ_{Y}).

$$\begin{aligned}\gamma &= \frac{E_{\text{interf}}(N_{\text{Al}}, N_{\text{O}}, N_{\text{Y}}) - E_{\text{bulk}}(N_{\text{Al}}, N_{\text{O}}, N_{\text{Y}})}{A_{\text{interf}}} \\ &= \frac{\Delta G_{\text{interf},\Gamma_{\text{Y}}=0} + N_{\text{Y}}(\Delta E^{\text{interf}}_{\text{defect,Y}} - \Delta E^{\text{bulk}}_{\text{defect,Y}})}{A_{\text{interf}}} \\ &= \gamma_{\Gamma_{\text{Y}}=0} + \frac{N_{\text{Y}}\Delta H_{\text{seg,Y}}}{A_{\text{interf}}} = \gamma_{\Gamma_{\text{Y}}=0} + \Gamma_{\text{Y}}\Delta H_{\text{seg,Y}}\end{aligned} \tag{3}$$

The bulk defect formation energy has been calculated with the CASCADE[47] code using a Mott–Littleton method,[48] which calculates the energy of an isolated dopant in an infinite bulk crystal. This is a good approximation for the low bulk concentrations studied, where dopant-dopant interactions are likely to be negligible. Equilibrium crystal morphologies for these surface energies could then be determined by the classic Wulff-construction[49] technique.

For comparison with bulk concentrations the surface cationic ratio x_{s} (Eq. (4)) can be defined, which is dependent on the considered interface depth (d_{interf}), making it necessary to take into account this value when comparing the values of x_{s}:

$$x_{\text{s}} = \frac{\Gamma_{\text{Y}}}{\Gamma_{\text{Al}}} \propto \frac{1}{d_{\text{interf}}} \tag{4}$$

The Y/Al ratios in bulk and interface (x_{b} and x_{s}) can be linked, after Mackrodt and Tasker,[50] with the help of the following equation:

$$\frac{x_{\text{s}}}{x_{\text{b}}} = \text{e}^{-\frac{\Delta H_{\text{seg}} + \frac{dH_{\text{seg}}}{dx_{\text{s}}} x_{\text{s}}(x_{\text{s}}+1)}{RT}} = C(x_{\text{s}}, T)\text{e}^{-\frac{\Delta H_{\text{seg}}}{RT}} \tag{5}$$

where R is the ideal gas constant, T is the temperature in Kelvin, and $\Delta H_{\text{seg}} = E_{\text{Y,interf}} - E_{\text{Y,bulk}}$ is the heat of segregation, the contribution of the vibrational entropy being neglected. If experimental measurements of $x_{\text{s}}/x_{\text{b}}$ are compared with theoretically calculated values of $\text{e}^{-\frac{\Delta H_{\text{seg}}}{RT}}$ the factor $C(x_{\text{s}}, T)$ can be empirically estimated for a given dopant concentration and temperature. The C factor incorporates the contribution of configurational entropy and the change in enthalpy of segregation as a function of surface coverage.

Another interesting quantity is the interface concentration in equilibrium with YAG second phase particles $\Gamma_{\text{Y,eq}}$. Owing to the equilibrium condition, this concentration is found where the energy of an Y atom at the interface is equivalent to its energy in the YAG phase[51] as given in the following equation:

$$\Delta H_{\text{sol}} = E_{\text{Y,interf}} - E_{\text{Y,YAG}} \overset{\text{eq.}}{=} 0 \tag{6}$$

In order to characterize the atomic structure at the interface, coordination numbers (CN) have been determined by counting the number of atoms within a cutoff radius[16] of Y–O: 2.9 Å, Al–O: 2.2 Å, Y–Y: 5.8 Å, and Y–Al: 4.225 Å.

III. Results and Discussion

(1) Structural Features of Y-Doped Interfaces

(A) Validation of Calculated Structures: The calculated structures have been compared with previously reported *ab initio* calculations for surfaces[52] and the Σ3 (10.0)[35] and Σ7 (01.2)[30] grain boundaries, respectively. For the case of the Σ7 (01.2) boundary the current model agrees with the *ab initio* calculations[30] on the fact that the "vacancy terminated" interface plane with a lateral translation of a half-cell perpendicular to the image plane ([$\bar{1}$2.0]direction) yields the lowest interfacial energy. Upon visual inspection the structures (Fig. 1) are found to be nearly equivalent to the ones shown in the cited references. As the authors kindly provided us with atomic coordinates for the Σ3 (10.0) and Σ7 (01.2) grain boundaries a quantitative comparison with these structures was possible. The current

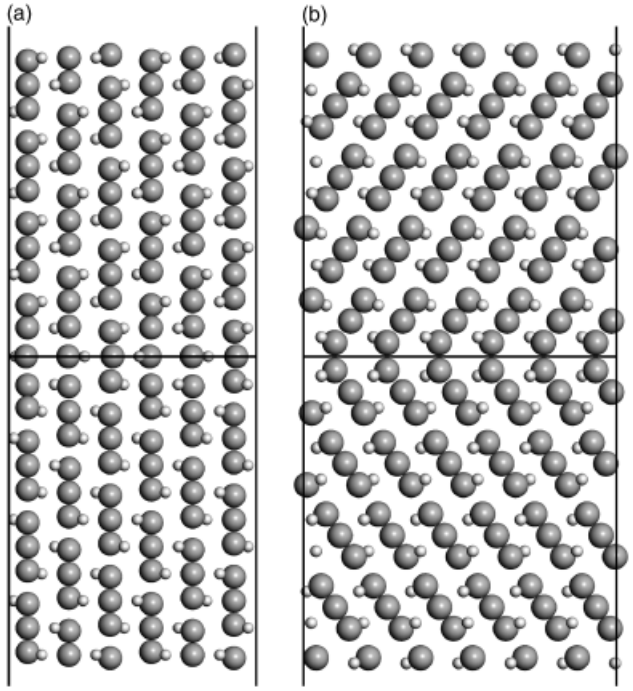

Fig. 1. Calculated interface structures (small light, Al; large dark, O) for (a) the Σ3 (10.0) grain boundary and (b) the Σ7 (01.2) grain boundary. The structures compare very well with those calculated using *ab initio* methods[30,35] for both boundaries.

Table II. Quantitative Comparison between Atomic Positions Calculated Using First Principle Methods by Fabris and Elsässer[35] as well as Marinopoulos and Elsässer[30] with Those Obtained with the Current Method

	Δx		Δy		Δz		Total offset			
Interface	Maximum	σ	Maximum	σ	Maximum	σ	Minimum	Maximum	Average	σ
Σ3 (10.0)	0.051	0.027	0.058	0.032	0.272	0.154	0.019	0.273	0.135	0.081
Σ7 (01.2)	0.206	0.137	0.141	0.082	0.192	0.099	0.064	0.281	0.170	0.070

The maximum offset and the standard deviation of the offset along the Cartesian axes in the system is given (Δ*x*, Δ*y*, and Δ*z*) as well as the minimum, maximum, average, and standard deviation of the total offset. All values are in Å.

coordinate set has been translated in space so that the mean Δ*x*, Δ*y*, and Δ*z* calculated over all atoms in the boundary core were zero. This method results in an approximate overlap, for which the differences can be analyzed. As can be seen from the results in Table II, the differences are on average smaller than 0.2 Å. These relatively large numbers can be explained by the fact that as discussed above the potentials result in a dilatation of the structure along the *c*-axis, which is well reflected in the Δ*z* differences for the Σ3 boundary. In fact the maximal Δ*x* and Δ*y* differences are extremely small showing that the potentials reproduce the structure well except along the dilated direction. Furthermore the comparison showed a slight underestimation of some of the Al–O bond lengths by the potential method, which will also contribute to a small but systematic difference.

In one instance direct comparison with experimental HRTEM results was possible: Richter and Rühle observed broken mirror symmetry at the Σ11 (10.1) interface viewed along the [10.2] direction. They related this to a relative shift by one half-cell of one half-crystal with respect to the other[53] which is consistent with the present calculations. Visual inspection (Fig. 2) confirms the very good agreement of the structure reported by Richter and Rühle and the present results.

The resulting structures thus seem to be well represented when compared with higher precision theoretical methods as well as experiment, placing the present method in between these two techniques although a validation for more cases would be desirable. Owing to its capacity to calculate a relatively high number of different grain boundaries, the method applied in the present work can serve to create a link between the highly accurate but also computationally expensive first principle methods and a grain-boundary population as observed by experiment in a ceramic microstructure.

(B) Interface Depth: Figure 3 shows ΔH_{seg} for single Y^{3+} ions as a function of depth from the interface plane, the heat of segregation being of the same order as reported previously.[23,34,35] The most favorable Y atom positions seem to be within 3 Å of the surfaces (Fig. 3(a)) and grain boundaries (Fig. 3(b)). Consequently the depth of the interface was chosen to be 3 Å for surfaces (d_{surf}) and 6 Å for grain boundaries (d_{GB}). There seems to be a trend of narrower Y segregation layers for low energy interfaces such as (01.2) and (00.1) surfaces or the Σ7 (01.2) grain boundary. The calculated depth of the interface d_{interf} seems to be consistent with the width (3–6 Å[17] and 1.5 Å[6]) of the structurally distorted region of grain boundaries in Y-doped α-alumina observed by HRTEM. Oversized Y ions (ionic radius of Y^{3+} 0.90 Å compared with Al^{3+} 0.54 Å) are likely to be found in the structurally distorted region as take up is facilitated due to the less dense structure as well as better strain relaxation as was observed by HRTEM. The calculated values are thus reasonable and most likely the interface depth of ~20 Å evaluated by chemical composition profiles[54] is too large due to the spatial resolution of the employed techniques (EDX and EELS). Consequently x_s values experimentally determined by these techniques might be too low (cf. Eq. (4)).

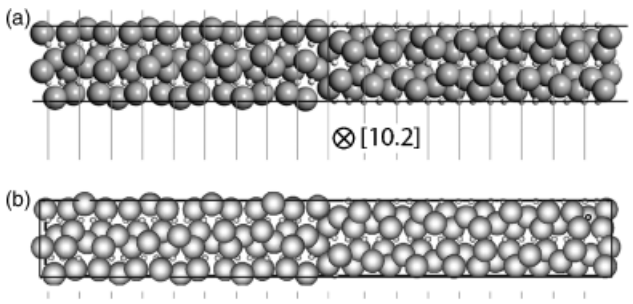

Fig. 2. Σ11 (10.1) interface viewed along the [10.2] direction (a) from our calculations (small light, Al; large dark, O) and (b) extracted with permission from Richter and Rühle[53] reproduced with kind permission of Springer Science and Business Media.

(C) Minimum Segregation Energy: The variation in enthalpy of solution as a function of the dopant concentration is reported for the examples of the (11.0) surface (Fig. 4(a)) and the Σ13 (11.3) grain boundary (Fig. 4(b)). As for most concentrations there is a configuration with a considerably lower energy, it has been assumed that most Y ions adopt this most favorable arrangement and segregation and solution energies depend solely on the energy of that configuration. It is interesting that the enthalpy of solution of the Y ions does not continuously increase with increasing Y concentration for either the surface or the grain boundary (Fig. 4). For many interfaces the energy decreases with increasing concentration until a value $\Gamma_{E_{min}}$ is reached for which the enthalpy of solution of the Y ions is minimal. The values of $\Gamma_{E_{min}}$ are reported in Table III for surfaces and in Table IV for grain boundaries. Many of the structures corresponding to a $\Gamma_{E_{min}}$ concentration are very particular, the Y ions forming geometric patterns at the interface by replacing an entire Al column or forming a diagonal pattern (Fig. 5). The coordination numbers and mean atom-atom distances for the most pronounced minima are listed in Table V. In most cases the Y atoms are positioned equidistantly and coordination numbers seem to be similar or even identical for all Y ions. The formation of Y columns at a Σ31 pure tilt grain boundary has been observed previously by Buban *et al.*[16] and Mackrodt and Tasker[50] found an energy minimum in the segregation energy curve of a (10.2) surface. However, a connection between energy minima and the formation of dopant patterns generated by Y ordering has not been reported by either group. One possibility put forward by Mackrodt and Tasker is the formation of an interface layer with second phase-like properties. The coordination numbers and mean atom–atom distances of such a layer would supposedly be similar to that of a second phase. Therefore the structural characteristics of the most pronounced minima have been compared with possible second phases (Y_2O_3 and YAG). There is, however, no striking correspondence. Namely Y–Y distances are much too large for any possible second phase (Table V), including $Y_4Al_2O_9$: 3.728 Å and $YAlO_3$: 3.722 Å.[8] It seems therefore that the observed ordering is caused by the structure of the particular interface rather than by the formation of a second phase-like layer.

Whatever the cause, the negative slope at the left of the curves in Fig. 4 indicates a positive interaction of Y ions at low interface concentrations as already observed by Exner and Finnis[23] as well as Elsässer and Elsässer,[36] the magnitude of the observed interaction agreeing well with the change of 0.2 eV per pair reported by the latter. At these concentrations, an inhomogeneous interface concentration caused by the clustering of the Y ions, might be possible and has also been experimentally observed.[8,17] Most authors, however, report no variation of Y concentration

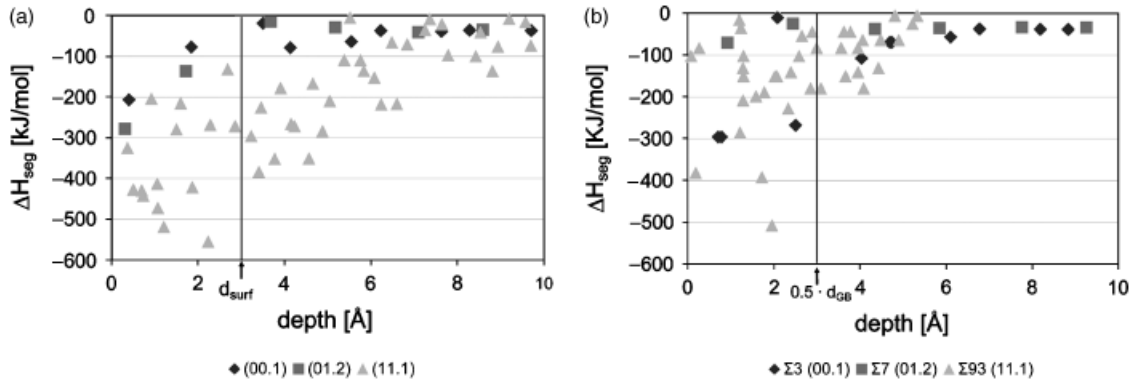

Fig. 3. Interface depth for (a) surfaces (b) and grain boundaries, shown on a plot of the enthalpy of segregation for single yttrium dopant sites situated at different depths in the structure.

along a single grain boundary, indicating that the described behavior might be limited to a few surfaces and special grain boundaries. A reason for this could be that clustering will be counteracted by entropy and will depend on the slope, i.e., the magnitude of the positive Y–Y interactions, which may be higher in special grain boundaries. Another explanation could be that most experimental measurements are carried out at Y saturation and as the clustering behavior is limited to Y interface concentrations lower than $\Gamma_{E_{min}}$ it might only be detectable at lower Y concentration.

The formation of Y columns or lines might also have an influence on the diffusion at the interface. For a cation-vacancy to pass the Y-ordered region the ordering has either to be disrupted or circumvented by a path leading away from the interface both likely to increase the associated energy barrier. Diffusion would thus not be affected parallel to the Y lines, but in particular cation diffusion is likely to be slowed in the perpendicular direction, leading to anisotropic diffusion in the interface. One of the proposed creep mechanisms is interface diffusion,[2,33] and consequently the creep resistance of Y-doped α-alumina might be enhanced by the formation of Y ordering at the interfaces, giving one possible explanation of the so-called Y effect.

(D) Equilibrium Interface Concentrations: The equilibrium interface concentration Γ_{eq} was calculated to be 0–6.64 Y/nm^2 for surfaces (Table III) and 0–5.19 Y/nm^2 for grain boundaries (Table IV). $\Gamma_{eq,GB}$ values reported in literature[7,8] vary between 3 and 6 Y/nm^2. The solubility seems to be highly dependent on the orientation of the interface. In general high energy interfaces seem to be able to accommodate more Y and the solubility is higher for surfaces than for grain boundaries. The dependence of the Y solubility on the orientation of the interface has been reported by several authors[6,11,12] with Y concentrations of 0–6 Y/nm^2 for the different grain boundaries. Most of these measurements observed general grain boundaries with the exception of the HRTEM work by Gemming *et al.*[17] which focused on mirror twin bicrystals, among them a Σ3 (10.0) bicrystal where no Y was detected. Again this is consistent with current simulation results (Table IV) where three grain boundaries are predicted not to accommodate any Y. Analysis of a specimen with random interfaces showed Σ3 (00.1) twins as well as Σ7 (01.2) twins; however, no Y was detected on either of these interfaces.[6] This is not entirely consistent with the present results which indicate that Y ions are likely to segregate to Σ3 (00.1) but not to Σ7 (01.2) boundaries. However, the authors themselves state that there was strong evidence that the studied Σ3 (00.1) were formed by deformation and that it was therefore likely that the segregation process was not completed as diffusion processes involved were too slow.

The calculated mean Γ_{eq} values are considerably lower than experimental results,[7,8] which is to be expected as more than half of the simulated interfaces are highly special, low energy interfaces whereas in alumina microstructures $<5\%$ of the interfaces were shown to be special.[6,9] As low energy interfaces do not accommodate Y ions as readily, the calculated Γ_{eq} mean values are likely to underestimate the concentration of dopants found at general grain boundaries in a sintered ceramic.

During sintering most surfaces are transformed into grain boundaries, which followed by grain growth reduces the specific interface area by more than half. As Γ_{eq} is much higher for surfaces than for grain boundaries, the nominal solubility of Y in the powder is much higher than the one in the sintered material. Inverse segregation involving diffusion of Y ions away from the interfaces and into the bulk is necessary if grain-boundary supersaturation levels leading to precipitation are to be avoided. As this process needs time extreme care has to be taken in controlling sintering speed and dopant concentration if YAG precipitation during sintering is to be avoided especially for rapid sintering by techniques such as spark plasma sintering.

(E) Coordination Number: The Y–O coordination number (CN) and the mean Y–O distance have been calculated for a

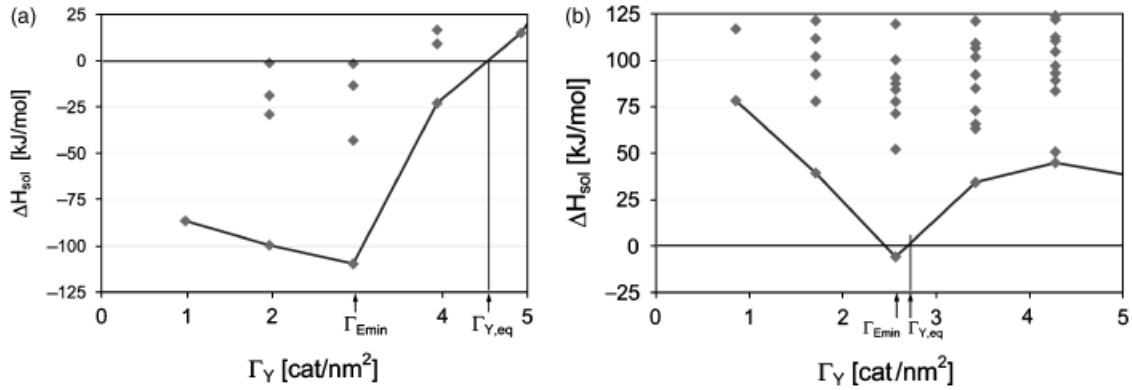

Fig. 4. Enthalpies of solution for increasing Y concentration at (a) the (11.0) surface and (b) the Σ13 (11.3) grain boundary (b). The coverage where the enthalpy of solution is minimal (Γ_{Emin}) is indicated as well as the equilibrium coverage ($\Gamma_{Y,eq}$) where the enthalpy of solution is zero.

Table III. Surface Energies (γ) and Relative Surface Energies (γ_{rel}) for Undoped and Doped Alumina

Surface miller indices (*hk.m*)	Pure Al_2O_3		10 ppm Y, 1600°C					General		Experiment	
	γ (J/m^2)	γ_{rel} (—)	Γ_Y (Y/nm^2)	Y–O (Å)	CN (—)	γ (J/m^2)	γ_{rel} (—)	$\Gamma_{Y,E_{min}}$ (Y/nm^2)	$\Gamma_{Y,eq}$ (Y/nm^2)	γ_{rel} (—)[55]	γ_{rel} (—)[56]
(00.1)	2.99	1.00	0.01	2.00	3.00	2.99	1.00	—	0.00	1.000	1.00
(01.2)	2.62	0.88	0.20	2.27	5.00	2.58	0.86	2.85	0.00	0.855	—
(11.3)	3.20	1.07	0.99	2.37	6.50	2.98	1.00	1.71	5.26	0.957	1.06
(11.0)	3.02	1.01	3.65	2.33	6.30	2.01	0.67	2.95	4.53	0.974	—
(10.0)	2.88	0.97	0.41	2.25	6.00	2.80	0.94	—	0.00	>1.008	—
(10.1)	3.67	1.23	3.69	2.31	5.36	2.68	0.90	3.24	6.12	0.947	1.07
(22.3)	3.18	1.06	3.22	2.31	5.82	2.32	0.78	—	3.79	—	—
(11.1)	3.48	1.17	5.12	2.25	5.19	2.04	0.68	—	6.64	—	—
Average	3.13	—	2.16	2.26	5.40	2.55	—	2.69	3.29	—	—

Also reported are the surface concentration (Γ_Y) as well as mean Y–O atom distances and Y–O coordination numbers (CN) in the doped case. The surface concentration with the minimal solution enthalpy ($\Gamma_{Y,E_{min}}$) as well as the one where the solution enthalpy is zero ($\Gamma_{Y,eq}$) are also reported. As a comparison the surface energies determined experimentally by Kitayama and Glaeser[55] for pure sapphire (impurities 15 ppm Si, 7 ppm Na, 6 ppm Mg, 2 ppm K, and 1 ppm Ca) as well as Choi *et al.*[56] for pure sapphire (impurities unknown) are given.

material in equilibrium with YAG precipitates (Γ_{eq}) and for a material with a bulk Y concentration of 10 ppm at a temperature of 1600°C. For surfaces CN varies between 3.00 and 5.82 and Y–O distances vary between 2.00 and 2.37 Å (Table III) whereas for grain boundaries CN varies between 6.51 and 7.49 and Y–O distances vary between 2.30 and 2.40 Å (Table IV), reflecting the undercoordinated environment at the surface leading to an increased bond-strength and as a result smaller Y–O distances.

On one hand, the Y–O coordination number and distance for surfaces are consistent with EXAFS measurements (CN = 4.8, Y–O = 2.33 Å).[8] On the other hand, the calculated CN values for grain boundaries are higher than the values reported by the same authors (CN = 4.2 for $\Gamma \sim 3$ Y/nm^2 and CN = 5.0 for $\Gamma \sim 5$ Y/nm^2, Y–O = 2.3 Å). Other theoretical studies also found higher coordination numbers of 6–7.[16,35] The Y–O distances in a sintered material (2.30 Å) are reasonably consistent with current results (2.37 Å). It should be noted that the standard deviation of the calculated Y–O distances within one interface is relatively large (Table V) indicating considerable structural distortions. Even for the highly ordered Σ3 (00.1) interface, the standard deviation is 0.253 Å which is large compared with the calculated value of 0.070 Å in bulk alumina. A smaller variation is observed from interface to interface. Consequently, the EXAFS measurements on a whole α-alumina sample are the result of a mixture of Y–O distances with a comparatively high variance, making the EXAFS features less distinct and underestimating the coordination numbers as mentioned previously.[15] Moreover because the powders used for surface measurements[8] were exposed to ambient air, surface hydroxylation is likely[52] which will change the chemical environment of the Y ions allowing only limited comparison between calculated and experimental results.

An energy loss near edge structure study showed some of the Y ions to have a noncentrosymmetric environment indicating that at least a fraction of the Y ions have nearest-neighbor oxygen atoms arranged in a tetrahedral configuration.[15] The current calculations did not reveal a tendency of oxygen ions to adopt a tetrahedral configuration around Y ions as the preferred Y–O coordination number seems to be seven as was also reported previously.[16] The exact position of the seven oxygen atoms seems to be strongly dependent on the grain-boundary structure (cf. Fig. 5).

(2) Energies of Y-Doped Interfaces

In the present article the factor $C(x_s, T)$ taking into account the concentration dependence of the heat of segregation (cf. Eq. (5)) has been evaluated by fitting to available experimental data. Considering a bulk concentration of 10 ppm an average $C(x_s, T)$ could be determined by fitting $\langle x_s \rangle = C(x_s, T) x_b \langle e^{-\Delta H/(RT)} \rangle$ to experimentally measured x_s values reported for the same bulk concentration.[3] $C(x_s, T)$ does not seem to vary much in the studied temperature range and a fairly good agreement between experimental and calculated values can be obtained for $C = 1.004 \times 10^{-5}$ for the entire temperature range (1600°–1800°C, Fig. 6).

Even if this method gives acceptable results, there are several points to bear in mind: first of all the calculated C factor is an average over different surfaces. The effective C factors may vary from surface to surface and are generally higher for low energy surfaces, having low Y concentrations, than for higher energy surfaces. Secondly the surfaces calculated in the present work represent only a subset of all possible surfaces likely to appear in experiment. Another point is that the experimental x_s values used for fitting take into account a surface segregation layer d_{surf}

Table IV. Interfacial Energies (γ) for Undoped and Doped Grain Boundaries

GB miller indices (*hk.m*)	Pure Al_2O_3		10 ppm Y, 1600°C					General			
	γ (J/m^2)	$\Delta\gamma$ (J/m^2)	Γ_Y (Y/nm^2)	Y–O (Å)	CN (—)	γ (J/m^2)	$\Delta\gamma$ (J/m^2)	$\Gamma_{Y,E_{min}}$ (Y/nm^2)	$\Gamma_{Y,eq}$ (Y/nm^2)	Y–O_{eq} (Å)	CN_{eq} (—)
Σ3 (00.1)	2.66	3.31	0.45	2.40	7.00	2.32	3.65	5.19	~5.19	2.40	7.00
Σ7 (01.2)	0.27	4.96	0.00	—	—	0.27	4.89	5.70	0.00	—	—
Σ3 (10.0)	0.50	5.27	0.00	—	—	0.50	5.11	13.64	0.00	—	—
Σ11 (10.1)	1.88	5.46	0.00	—	—	1.88	3.47	9.72	0.00	—	—
Σ13 (11.3)	2.42	3.99	0.96	2.36	7.00	2.22	3.74	2.57	2.69	2.36	7.00
Σ43 (22.3)	2.95	3.40	1.79	2.35	7.07	2.54	2.10	0.95	2.93	2.30	6.51
Σ93 (11.1)	2.87	4.09	3.23	2.36	7.39	2.10	1.98	—	3.83	2.37	7.49
Average	1.94	4.35	0.92	2.37	7.12	1.69	3.56	6.29	2.09	2.36	7.00

Also given is the gain in interfacial energy ($\Delta\gamma$) when forming a grain boundary from two surfaces. The interfacial concentration at 10 ppm Y at 1600°C is given (Γ_Y), the mean Y–O atom distances at the interface and the coordination number of Y–O (CN). The interfacial concentration at which the interfacial energy is minimal is $\Gamma_{Y,E_{min}}$ and the interfacial energy at zero solution enthalpy is ($\Gamma_{Y,eq}$). For the case where the grain boundary dopants concentration is in equilibrium with a second phase the Y–O bond length and the Y-coordination numbers are also reported.

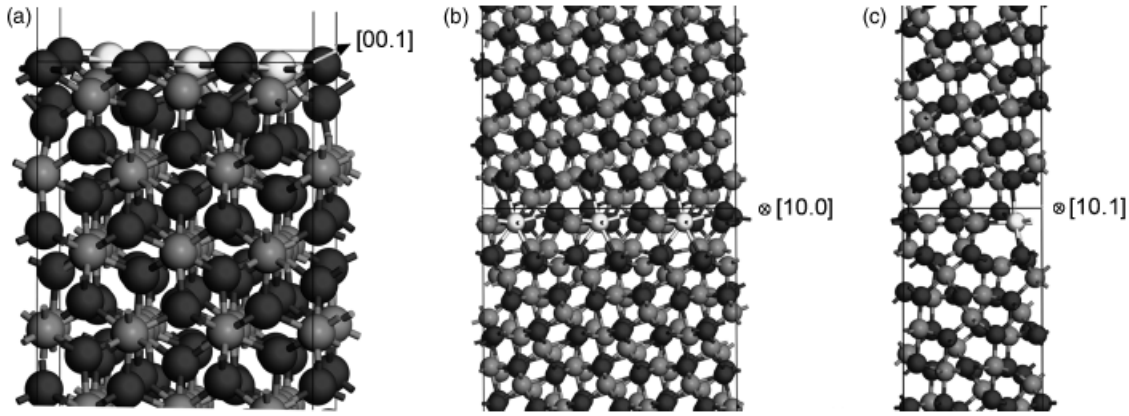

Fig. 5. Formation of Y patterns and columns at surfaces and grain boundaries: (a) (11.0) surface at $\Gamma_Y = 2.95$ Y/nm^2 and (b) Σ13 (11.3) grain boundary at $\Gamma_Y = 2.57$ Y/nm^2 viewed along [10.0] and (c) along [10.1].

much larger then 3 Å, which is likely to influence $C(x_s, T)$. This error introduced in $C(x_s, T)$ would also explain the considerably lower predicted average surface concentration ($\Gamma_Y = 2.16$ nm^{-2}) at the bulk solubility limit of 10 ppm when compared with the one calculated in equilibrium with YAG particles ($\Gamma_{Y,eq} = 3.29$ nm^{-2}). Although the experimental data seems to support our results, YAG precipitation was observed at 10 ppm and temperatures above 1900°C.[3] Last but not least, Eq. (4) assumes all configurations of Y ions at the interface to have the same energy and therefore to be adopted with the same probability. This is evidently not the case as illustrated in Fig. 4 and consequently entropic contributions are likely to lead to lower interface concentrations than predicted by Eq. (4). These limitations lead to the desire for a more fundamental approach, which to some degree take into account the effect of entropy. An approach is currently being developed and will be presented in a separate article.

With the value of C determined above (1.004×10^{-5}) the interface energies of α-alumina with a bulk concentration of 10 ppm Y at a temperature of 1600°C have been determined. The calculated surface energies are listed in Table III. For pristine surfaces the energies lie between 2.62 and 3.48 J/m^2 and between 2.01 and 2.99 J/m^2 for doped surfaces. The faces of the calculated undoped equilibrium morphology are the same as the faces found in experimental equilibrium morphologies[55] with two exceptions: firstly the calculated equilibrium shape has small (22.3) surfaces, which were not experimentally observed, and secondly the (10.1) surfaces of the experimental equilibrium morphology have been replaced by (10.0) surfaces in the calculated results. Comparing the relative surface energies obtained in this work with the experimental references it is striking that the (00.1) surface is predicted to be very unstable, only the (10.0) surface having an even higher surface energy.[55] Other data, however, predict the (00.1) basal plane to be the most stable within the set of surfaces treated in that study.[56] This second result is compatible with the current findings, the surface energies matching reasonably well. The discrepancy in the results may come from the impurity content in the alumina samples, the simulations being carried out for 100% pure alumina.

The influence of Y segregation on surface energies is considerable as can be seen from the mean surface energy change from 3.13 to 2.55 J/m^2 upon introduction of 10 ppm Y in the bulk. Because, as seen above, higher energy surfaces are more favorable to Y segregation the equilibrium morphology changes significantly (Fig. 7). It has to be noted that the actual equilibrium morphology of a Y-doped α-alumina might be slightly different from Fig. 7(b) as the number of studied surfaces may be insufficient for a completely reliable prediction.

The calculated grain-boundary energies are listed in Table IV. The energies lie between 0.27 and 2.95 J/m^2 for pristine grain boundaries and between 0.27 and 2.54 J/m^2 for Y-doped interfaces. The grain-boundary energy for the Σ3 (00.1) and Σ7 (01.2) can be compared with previous calculations. The basal twin lies in between the energies of 1.9 (*ab initio*) and 3.91 J/m^2 (empirical) reported by Marinopoulos *et al.*[28] whereas for the Σ7 (01.2) the current study gives a lower energy than the 0.63 J/m^2 previously reported by *ab initio* methods.[30] The present results agree with the general trend that basal twins have a considerably higher surface energy than rhombohedral (01.2) twin. One aspect not taken into account in the present work is the formation of intrinsic, such as Schottky defects at the grain boundary, which may contribute to a lowering of the interfacial energies. The influence of Y dopants on grain-boundary energies seems to be less important than on surface energies. The mean interface energy changes from 1.94 to 1.69 J/m^2 upon doping with 10 ppm Y at 1600°C.

In order to be able to estimate the influence of Y dopants on the sintering behavior, the energy difference between two separate surfaces and the corresponding grain boundary ($\Delta\gamma$) has been calculated which can be assumed to be the driving force for sintering. The mean value of $\Delta\gamma$ is 4.35 J/m^2 for pure and 3.56 J/m^2 for Y-doped α-alumina. The total influence of the presence of Y ions on

Table V. Comparison of the Coordination Numbers (CN), Mean Atom Distances and Standard Deviation of Atom Distance (σ) of Y–O, Y–Y, and Y–Al at the (11.0) Surface, the Σ13 (11.3) and Σ3 (00.1) Grain Boundaries at Y Concentrations Corresponding to $\Gamma_{Y,E_{min}}$

Interface	CN_{Y-O}	Y–O (Å)	σ_{Y-O} (Å)	CN_{Y-Y}	Y–Y (Å)	σ_{Y-Y} (Å)	CN_{Y-Al}	Y–Al (Å)	σ_{Y-Al} (Å)
(11.0)	7	2.399	0.223	2	4.959	3.77E−11	10	3.403	0.358
Σ13 (11.3)	7	2.356	0.151	2	4.959	1.07E−09	16	3.457	0.242
Σ3 (00.1)	7	2.400	0.253	6	4.719	6.05E−09	14	3.490	0.324
Mineral									
Y_2O_3[8]	6	2.284	—	12	3.757	—	—	—	—
YAG[8]	8	2.351	—	4	3.677	—	10	3.414	—

As a comparison the same numbers are given for pure yttrium oxide and yttrium–aluminum–garnet (YAG).

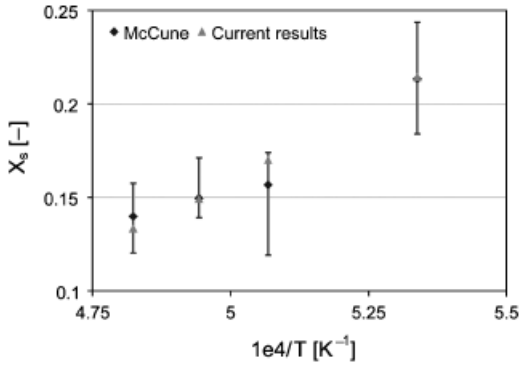

Fig. 6. Determination of the entropy factor C by fitting to data by McCune *et al.*[3]—agreement between calculated results (light triangles) and results reported by McCune (dark diamonds with error bars).

the interface energies of sintered α-alumina might be estimated by a mean energy value weighted by $\Delta\gamma$ as given in the following equation:

$$\gamma_{GB,w} = \frac{\sum(\gamma_{GB}\Delta\gamma_{GB})}{\sum\Delta\gamma_{GB}} \quad (7)$$

This will slightly over-emphasize the influence of Y as grain-boundary formation is not free but geometrically restricted depending on the relative position of the initial grains as well as on $\Delta\gamma$. The change due to Y doping is, however, not pronounced, the weighted mean value changing only from 1.79 to 1.47 J/m^2. This is consistent with the fact that the addition of Y does not have a considerable influence on the orientation of grain boundaries[9] nor does it effectively inhibit grain growth.[6,7] The mean value of $\Delta\gamma$, however, changes from 4.35 to 3.56 J/m^2. Together with a possible inhibition of diffusion parallel to the interfaces, due to the fact that Y ions enhance the cation–oxygen coordination at the grain boundaries[16] and may form barrier-like patterns, this gives a possible explanation for the retardation of the sintering process in presence Y dopant ions as observed experimentally.[10,57]

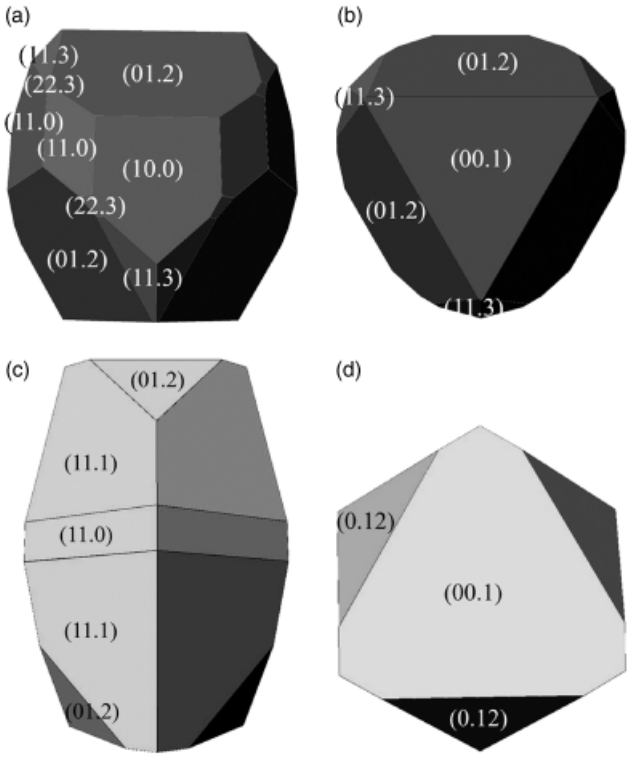

Fig. 7. Equilibrium morphologies of undoped α-alumina (a) front and (b) top view. Equilibrium morphologies of 10 ppm Y-doped α-alumina at 1600°C seen again from (c) front and (d) top view.

IV. Conclusions

The aim of the current work was to create a link between *ab initio* studies of isolated grain boundaries and experimental results obtained with a material containing a statistical population of interfaces. This has been attempted by using energy minimization techniques to look at eight different crystallographic surfaces and seven mirror twin grain boundaries. The most important findings are that at low Y concentrations interactions seem to exist between segregated Y ions on some interfaces, which lead to the formation of patterns due to Y ordering. These patterns may result in lower diffusion coefficients parallel to the interfaces, as they would have to be disrupted or contoured by diffusion processes both of which will be more energetic than undisturbed diffusion. The reduced diffusion coefficients could be one reason why Y doping reduces creep in alumina.

Surfaces seem to be able to accommodate more Y than grain boundaries. During sintering the conversion of surfaces to grain boundaries together with the reduction of the specific surface area is therefore prone to lead to YAG precipitation, especially if the sintering speed is too high to allow inverse segregation. The Y–O bond lengths at the interfaces are shown to be very variable which explains why EXAFS techniques are prone to underestimate Y–O coordination numbers in α-alumina. It has also been determined that segregation of Y ions might have an important influence on the surface energies and thus on the equilibrium morphology of α-alumina, the changes being especially marked at concentrations lower than saturation.

These overall findings, although on a limited number of low energy surfaces and grain boundaries, illustrate the potential of using energy minimization techniques to help in our understanding of interfacial phenomena at the atomistic level in ceramic materials. The calculation of a relatively high number of surfaces and grain boundaries allows getting an estimate of the segregation behavior in presence of a population of interfaces as would be observed in a powder or ceramic. Moreover the data developed here can be used to build microstructural models, which will then allow making the step toward describing not only segregation toward isolated grain boundaries but segregation within a ceramic microstructure.

Acknowledgments

We would like to thank Prof. Christian Elsässer for his important contribution to the validation of the model by providing the final atomic coordinates of his *ab initio* simulations.

References

[1]J. H. Cho, M. P. Harmer, H. M. Chan, J. M. Rickman, and A. M. Thompson, "Effect of Yttrium and Lanthanum on the Tensile Creep Behavior of Aluminum Oxide," *J. Am. Ceram. Soc.*, **80** [4] 1013–7 (1997).

[2]J. Cho, C. M. Wang, H. M. Chan, J. M. Rickman, and M. P. Harmer, "Role of Segregating Dopants on the Improved Creep Resistance of Aluminum Oxide," *Acta Mater.*, **47** [15–16] 4197–207 (1999).

[3]R. C. McCune, W. T. Donlon, and R. C. Ku, "Yttrium Segregation and YAG Precipitation at Surfaces of Yttrium-Doped α-Al_2O_3," *J. Am. Ceram. Soc.*, **69** [8] C196–9 (1986).

[4]J. D. Cawley and J. W. Halloran, "Dopant Distribution in Nominally Yttrium-Doped Sapphire," *J. Am. Ceram. Soc.*, **69** [8] C195–6 (1986).

[5]A. M. Thompson, K. K. Soni, H. M. Chan, M. P. Harmer, D. B. Williams, J. M. Chabala, and R. Levi-Setti, "Dopant Distributions in Rare-Earth-Doped Alumina," *J. Am. Ceram. Soc.*, **80** [2] 373–6 (1997).

[6]M. A. Gülgün, V. Putlayev, and M. Rühle, "Effects of Yttrium Doping α-Alumina: I, Microstructure and Microchemistry," *J. Am. Ceram. Soc.*, **82** [7] 1849–56 (1999).

[7]M. A. Gülgün, R. Voytovych, I. MacLaren, M. Rühle, and R. M. Cannon, "Cation Segregation in an Oxide Ceramic with Low Solubility: Yttrium Doped α-Alumina," *Interface Sci.*, **10** [1] 99–110 (2002).

[8]C. M. Wang, G. S. Cargill, H. M. Chan, and M. P. Harmer, "Structural Features of Y-Saturated and Supersaturated Grain Boundaries in Alumina," *Acta Mater.*, **48** [10] 2579–91 (2000).
[9]J. Cho, H. M. Chan, M. P. Harmer, and J. M. Rickman, "Influence of Yttrium Doping on Grain Misorientation in Aluminum Oxide," *J. Am. Ceram. Soc.*, **81** [11] 3001–4 (1998).
[10]E. Sato and C. Carry, "Yttria Doping and Sintering of Submicrometer-Grained α-Alumina," *J. Am. Ceram. Soc.*, **79** [8] 2156–60 (1996).
[11]M. J. Kim, Y. K. Cho, and D. Y. Yoon, "Kinked Grain Boundaries in Alumina Doped with Y_2O_3," *J. Am. Ceram. Soc.*, **87** [4] 717–9 (2004).
[12]D. Bouchet, F. Dupau, and S. Lartigue-Korinek, "Structure and Chemistry of Grain Boundaries in Yttria Doped Aluminas," *Microsc. Microanal. Microstruct.*, **4** [6] 561–73 (1993).
[13]W. Swiatnicki, S. Lartigue-Korinek, and J. Y. Laval, "Grain Boundary Structure and Intergranular Segregation in Al_2O_3," *Acta Metall. Mater.*, **43** [2] 795–805 (1995).
[14]C. M. Wang, G. S. Cargill, M. P. Harmer, H. M. Chan, and J. Cho, "Atomic Structural Environment of Grain Boundary Segregated Y and Zr in Creep Resistant Alumina from EXAFS," *Acta Mater.*, **47** [12] 3411–22 (1999).
[15]C. M. Wang, G. S. Cargill, H. M. Chan, and M. P. Harmer, "X-Ray Absorption Near-Edge Structure of Grain-Boundary-Segregated Y and Zr in Creep-Resistant Alumina," *J. Am. Ceram. Soc.*, **85** [10] 2492–8 (2002).
[16]J. P. Buban, K. Matsunaga, J. Chen, N. Shibata, W. Y. Ching, T. Yamamoto, and Y. Ikuhara, "Grain Boundary Strengthening in Alumina by Rare Earth Impurities," *Science*, **311** [5758] 212–5 (2006).
[17]T. Gemming, S. Nufer, W. Kurtz, and M. Rühle, "Structure and Chemistry of Symmetrical Tilt Grain Boundaries in α-Al_2O_3: II, Bicrystals with Y at the Interface," *J. Am. Ceram. Soc.*, **86** [4] 590–4 (2003).
[18]H. Yoshida, K. Matsunaga, T. Yamamoto, Y. Ikuhara, and T. Sakuma, "Dopant Effect on the High-Temperature Grain Boundary Sliding in Alumina," *Superplasticity Adv. Mater.*, **447–448**, 299–304 (2003).
[19]H. Yoshida, Y. Ikuhara, and T. Sakuma, "High Temperature Plastic Deformation Related to Grain Boundary Chemistry in Cation-Doped Alumina," *Mater. Sci. Eng. A—Struct. Mater. Prop. Microstruct. Proc.*, **387–389**, 723–7 (2004).
[20]Y. Ikuhara, T. Watanabe, T. Saito, H. Yoshida, and T. Sakuma, "Atomic Structure and Chemical Bonding State of Sapphire Bicrystal," *Intergranular Interphase Boundaries Mater.*, **294–296**, 273–6 (1999).
[21]H. Yoshida, Y. Ikuhara, and T. Sakuma, "Grain Boundary Electronic Structure and High-Temperature Plastic Flow in Polycrystalline Al_2O_3," *Adv. Ceram. Compos.*, **247**, 263–6 (2003).
[22]P. R. Kenway, "Calculated Structures and Energies of Grain Boundaries in α-Al_2O_3," *J. Am. Ceram. Soc.*, **77** [2] 349–55 (1994).
[23]M. Exner and M. W. Finnis, "Atomistic Simulation of Grain Boundaries in Alumina," *Intergranular Interphase Boundaries Mater.*, **207–209**, 225–8 (1996).
[24]H. Suzuki, H. Matsubara, J. Kishino, and T. Kondoh, "Simulation of Surface and Grain Boundary Properties of Alumina by Molecular Dynamics Method," *J. Ceram. Soc. Jpn.*, **106** [12] 1215–22 (1998).
[25]H. Suzuki and H. Matsubara, "Microstructural Design of Grain Boundaries in Alumina Based Ceramics," *Sci. Eng. Ceram. II*, **2**, 453–6 (1999).
[26]W. Wunderlich and H. Awaji, "Molecular Dynamics Simulation of Alumina Interfaces in Order to Design Advanced Materials," *Sci. Eng. Ceram. II*, **2**, 449–52 (1999).
[27]A. G. Marinopoulos and C. Elsässer, "Density-Functional and Shell-Model Calculations of the Energetics of Basal-Plane Stacking Faults in Sapphire," *Philos. Mag. Lett.*, **81** [5] 329–38 (2001).
[28]A. G. Marinopoulos, S. Nufer, and C. Elsässer, "Interfacial Structures and Energetics of Basal Twins in α-Al_2O_3: First-Principles Density-Functional and Empirical Calculations," *Phys. Rev. B*, **63** [16] 165112 (2001).
[29]S. Fabris, S. Nufer, C. Elsässer, and T. Gemming, "Prismatic Σ3 (10-10) Twin Boundary in α-Al_2O_3 Investigated by Density Functional Theory and Transmission Electron Microscopy," *Phys. Rev. B*, **66** [15] 155415 (2002).
[30]A. G. Marinopoulos and C. Elsässer, "Microscopic Structure and Bonding at the Rhombohedral Twin Interface in α-Al_2O_3," *Acta Mater.*, **48** [18–19] 4375–86 (2000).
[31]S. Fabris and C. Elsässer, "Σ13 (10-14) Twin in α-Al_2O_3: A Model for a General Grain Boundary," *Phys. Rev. B*, **64** [24] 245117 (2001).
[32]H. Nishimura, K. Matsunaga, T. Saito, T. Yamamoto, and Y. Ikuhara, "Atomic Structures and Energies of Σ7 Symmetrical Tilt Grain Boundaries in Alumina Bicrystals," *J. Am. Ceram. Soc.*, **86** [4] 574–80 (2003).
[33]J. Chen, L. Z. Ouyang, and W. Y. Ching, "Molecular Dynamics Simulation of Y-Doped Σ37 Grain Boundary in Alumina," *Acta Mater.*, **53** [15] 4111–20 (2005).
[34]C. Elsässer and A. G. Marinopoulos, "Substitutional Cation Impurities in α-Al_2O_3: Ab-Initio Case Study of Segregation to the Rhombohedral Twin Boundary," *Acta Mater.*, **49** [15] 2951–9 (2001).
[35]S. Fabris and C. Elsässer, "First-Principles Analysis of Cation Segregation at Grain Boundaries in α-Al_2O_3," *Acta Mater.*, **51** [1] 71–86 (2003).
[36]C. Elsässer and T. Elsässer, "Codoping and Grain-Boundary Cosegregation of Substitutional Cations in α-Al_2O_3: A Density–Functional–Theory Study," *J. Am. Ceram. Soc.*, **88** [1] 1–14 (2005).
[37]W. Y. Ching, J. Chen, P. Rulis, L. Ouyang, and A. Misra, "Ab Initio Modeling of Clean and Y-Doped Grain Boundaries in Alumina and Intergranular Glassy Films (IGF) in β-Si_3N_4," *J. Mater. Sci.*, **41** [16] 5061–7 (2006).
[38]G. W. Watson, E. T. Kelsey, N. H. deLeeuw, D. J. Harris, and S. C. Parker, "Atomistic Simulation of Dislocations, Surfaces and Interfaces in MgO," *J. Chem. Soc.-Faraday Trans.*, **92** [3] 433–8 (1996).
[39]G. V. Lewis and C. R. A. Catlow, "Potential Models for Ionic Oxides," *J. Phys. C—Solid State Phys.*, **18** [6] 1149–61 (1985).
[40]B. G. Dick and A. W. Overhauser, "Theory of the Dielectric Constants of Alkali Halide Crystals," *Phys. Rev.*, **112** [1] 90–103 (1958).
[41]M. J. Davies, P. R. Kenway, P. J. Lawrence, S. C. Parker, W. C. Mackrodt, and P. W. Tasker, "Impurity Segregation to the Surfaces of Corundum-Structured Oxides," *J. Chem. Soc.-Faraday Trans. 2*, **85** [5] 555–63 (1989).
[42]D. J. Cooke, S. E. Redfern, and S. C. Parker, "Atomistic Simulation of the Structure and Segregation to the (0001) and (01-12) Surfaces of Fe_2O_3," *Phys. Chem. Miner.*, **31** [8] 507–17 (2004).
[43]M. Wilson, M. Exner, Y. M. Huang, and M. W. Finnis, "Transferable Model for the Atomistic Simulation of Al_2O_3," *Phys. Rev. B*, **54** [22] 15683–9 (1996).
[44]T. S. Bush, J. D. Gale, C. R. A. Catlow, and P. D. Battle, "Self-Consistent Interatomic Potentials for the Simulation of Binary and Ternary Oxides," *J. Mater. Chem.*, **4** [6] 831–7 (1994).
[45]M. Blanchard, K. Wright, and J. D. Gale, "Atomistic Simulation of Mg_2SiO_4 and Mg_2GeO_4 Spinels: A New Model," *Phys. Chem. Miner.*, **32** [5–6] 332–8 (2005).
[46]J. D. Gale, "GULP: A Computer Program for the Symmetry-Adapted Simulation of Solids," *J. Chem. Soc.-Faraday Trans.*, **93** [4] 629–37 (1997).
[47]M. Leslie, "Cascade"; In Daresbury Laboratory Report DL/SCI-TM31T 1981.
[48]M. F. Mott and M. J. Littleton, "Conduction in Polar Crystals. I. Electrolytic Conduction in Solid Salts," *Trans. Faraday Soc.*, **34** [1] 485–99 (1938).
[49]G. Wulff, "On the Question of Speed of Growth and Dissolution of Crystal Surfaces," *Zeitschrift Krystallogr. Mineral.*, **34** [5/6] 449–530 (1901).
[50]W. C. Mackrodt and P. W. Tasker, "Segregation Isotherms at the Surfaces of Oxides," *J. Am. Ceram. Soc.*, **72** [9] 1576–83 (1989).
[51]U. Aschauer, P. Bowen, and S. C. Parker, "Atomistic Modeling Study of Surface Segregation in Nd:YAG," *J. Am. Ceram. Soc.*, **89** [12] 3812–6 (2006).
[52]A. Marmier and S. C. Parker, "Ab Initio Morphology and Surface Thermodynamics of α-Al_2O_3," *Phys. Rev. B*, **69** [11] 115409 (2004).
[53]G. Richter and M. Rühle, "Quantitative HRTEM Investigations of a Symmetrical Tilt Σ11 Grain Boundary with Two Different Grain Boundary Planes in α-Al_2O_3," *Interface Sci.*, **12** [2–3] 197–211 (2004).
[54]J. Bruley, J. Cho, H. M. Chan, M. P. Harmer, and J. M. Rickman, "Scanning Transmission Electron Microscopy Analysis of Grain Boundaries in Creep-Resistant Yttrium- and Lanthanum-Doped Alumina Microstructures," *J. Am. Ceram. Soc.*, **82** [10] 2865–70 (1999).
[55]M. Kitayama and A. M. Glaeser, "The Wulff Shape of Alumina: III, Undoped Alumina," *J. Am. Ceram. Soc.*, **85** [3] 611–22 (2002).
[56]J. H. Choi, D. Y. Kim, B. J. Hockey, S. M. Wiederhorn, C. A. Handwerker, J. E. Blendell, W. C. Carter, and A. R. Roosen, "Equilibrium Shape of Internal Cavities in Sapphire," *J. Am. Ceram. Soc.*, **80** [1] 62–8 (1997).
[57]D. Prot, M. Le Gall, B. Lesage, A. M. Huntz, and C. Monty, "Self-Diffusion in α-Al_2O_3 IV. Oxygen Grain-Boundary Self-Diffusion in Undoped and Yttria-Doped Alumina Polycrystals," *Phil. Mag. A*, **73** [4] 935–49 (1996).
[58]R. S. Liu, W. C. Shi, Y. C. Cheng, and C. Y. Huang, "Crystal Structures and Peculiar Magnetic Properties of α- and γ-Al_2O_3 Powders," *Mod. Phys. Lett. B*, **11** [26–27] 1169–74 (1997).
[59]D. R. Lide, *CRC Handbook of Chemistry and Physics, 88th Edition (Internet Version 2008)*. CRC Press/Taylor and Francis, Boca Raton, FL, 2008. □